Fengcheng Pei, Lin Xiang, and Anja Klein, “Transmit Beamforming and Array Steering Optimization for UAV-Aided Bistatic ISAC” in *IEEE Global Communications Conference, Cape Town, South Africa, 2024.*

Transmit Beamforming and Array Steering Optimization for UAV-Aided Bistatic ISAC

Fengcheng Pei, Lin Xiang, and Anja Klein
Communications Engineering Lab, Technical University of Darmstadt, Germany
Email: {f.pei, l.xiang, a.klein}@nt.tu-darmstadt.de

***Abstract*—In this paper, we consider bistatic integrated sensing and communication (ISAC) enabled by an unmanned aerial vehicle (UAV) and a ground sensing receiver. The UAV employs a rotatable array of patch antennas to communicate with multiple ground users and simultaneously probe multiple targets, while using the same transmit signals. To minimize the UAV's load and transceiver complexity, the sensing receiver collects and processes echoes of the probing signals for e.g. detecting the activities of the targets. We jointly optimize transmit beamforming and array steering at the UAV to maximize the minimum received signal-to-interference-plus-noise ratio (SINR) for all targets while ensuring quality-of-service (QoS) for each communication user. Given the highly nonconvex nature of the formulated problem and the difficulty in obtaining its optimal solution, we propose a low-complexity suboptimal algorithm based on proximal block coordinate descent (BCD). This algorithm can exploit the underlying structure of the problem by decomposing it into several convex and manifold optimization subproblems, which are then alternately solved using off-the-shelf solvers. Simulation results demonstrate that by jointly optimizing transmit beamforming and array steering, the rotatble patch antenna array significantly enhances the sensing performance of UAV-aided bistatic ISAC while guaranteeing communication QoS, even in scenarios with limited number of transmit antennas and undesirable line-of-sight (LoS) interference from the ISAC transmitter.**

I. Introduction

Recent research has increasingly focused on exploiting multi-antenna unmanned aerial vehicles (UAVs) to provide on-demand integrated sensing and communication (ISAC) services [1]. Thanks to their agile mobility and rapid deployment capabilities, UAV-aided ISAC systems can enhance the performance of terrestrial sensing and communication services in the sixth-generation (6G) wireless networks, while also expanding network coverage in both standard and emergency scenarios [2]. However, unlike terrestrial ISAC systems, UAVs have unique channel characteristics, are usually constrained by their size, weight, and power (SWAP), and may accommodate only a limited number of antennas. Therefore, how to intelligently design and optimize multi-antenna transmission and reception for enabling efficient UAV-aided ISAC poses a substantial research challenge [3].

To overcome this challenge, several studies have investigated the joint optimization of beamforming and trajectory design for UAV-aided ISAC [4]–[6]. These studies leverage the UAV's three-dimensional (3D) mobility to enhance communication throughput while meeting quality-of-service (QoS) requirements for sensing. However, they primarily consider arrays of isotropic antennas, overlooking the 3D radiation patterns of practical antennas. In contrast, our research in [7] and [8] investigate a rotatable array of directional antennas, including half-wavelength dipoles and patch antennas, for UAV-aided communication and sensing. Unlike [4]–[6], we utilize the UAV's movement or an onboard gimbal to mechanically steer/rotate the antenna array in 3D space. By exploiting these additional spatial degrees of freedom (DoFs), we jointly optimize array steering and beamforming to maximize the communication and sensing performance in [7], [8].

However, the aforementioned studies [4]–[8] have focused on monostatic ISAC, which relies on advanced full-duplex transceivers equipped with sophisticated self-interference cancellation hardware or software [9]. Bistatic ISAC, which separates the transmitter and receiver into distinct nodes, offers a compelling alternative. This separation not only simplifies the ISAC transceiver design, but also relieves the UAV's load and increases system flexibility, making it a more viable solution for UAVs. Nevertheless, as the UAV is elevated, undesirable line-of-sight (LoS) interference between the ISAC transmitter and receiver may jeopardize the system performance. To counteract this, adaptive filtering and signal processing techniques have been suggested in the radar literature [10] to effectively mitigate such interference.

In this paper, we address the challenges of UAV-aided bistatic ISAC by employing a rotatable array of patch antennas onboard the UAV for advanced ISAC signal transmission [7], [8]. Through adaptive transmit beamforming and array steering, the patch array can generate highly directive beams to focus the signal energy towards the desired directions, while minimizing interference leaked towards the sensing receiver. To maximize the benefits of our proposed scheme, we jointly optimize transmit beamforming and 3D steering of the rotatable patch array to maximize the minimal signal-to-interference-plus-noise ratio (SINR) at the sensing receiver while ensuring QoS for multiple communication users. Due to the directional radiation pattern of patch antennas and the complex fractional objective function, the resulting optimization problem is highly nonconvex and more difficult to solve than those in [7], [8]. By exploring the underlying problem structure, we decompose the problem into manifold and convex optimization subproblems, which are further solved using a low-complexity iterative algorithm. Our contributions are:

- We investigate advanced ISAC signal transmission for UAV-aided bistatic ISAC by utilizing a rotatable array of patch antennas onboard the UAV.
- We formulate a nononvex problem to jointly optimize the transmit beamforming and array steering for maximizing the minimum received SINR of all targets at the sensing receiver while ensuring QoS for each communication user. We further propose a low-complexity proximal block

This work has been funded by the LOEWE initiative (Hesse, Germany) within the emergenCITY center under grant LOEWE/1/12/519/03/05.001(0016)/72 and has been supported by the BMBF project Open6GHub under grant 16KISKO14 and by DAAD with funds from the German Federal Ministry of Education and Research (BMBF).

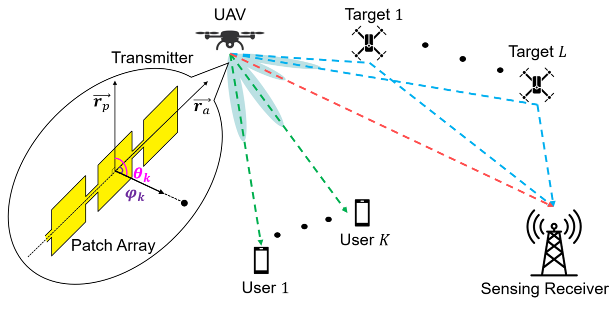

Fig. 1. System model of UAV-aided ISAC with bistatic radar deployment.

coordinate descent (BCD) method to solve it.

- Simulation results show that joint transmit beamforming and array steering using the rotatable patch array can effectively mitigate interference and significantly improve the sensing and communication performance for UAV-aided bistatic ISAC.

In the remainder of this paper, Section II introduces the system model for UAV-aided bistatic ISAC. The joint beamforming and steering optimization problem is formulated and solved in Sections III and IV, respectively. Section V presents the simulation results and finally, Section VI concludes the paper.

Notation: Throughout this paper, matrices and vectors are denoted by boldface capital and lower-case letters, respectively. $\mathbb{C}^{m\times n}$ and $\mathbb{R}^{m\times n}$ denote $m \times n$ complex- and real-valued matrices, respectively. $\boldsymbol{I}_M$ is the $M \times M$ identity matrix. $j = \sqrt{-1}$ is the imaginary unit of complex numbers and $\|\cdot\|$ is the l_2-norm of a vector. $\boldsymbol{A}^T$ and $\boldsymbol{A}^H$ are the transpose and complex conjugate transpose of matrix $\boldsymbol{A}$, respectively. $\mathrm{tr}(\boldsymbol{A})$ and $\mathrm{rank}(\boldsymbol{A})$ denote the trace and rank of matrix $\boldsymbol{A}$, respectively. Finally, $\overrightarrow{\boldsymbol{a}}$ denotes a unit direction vector.

II. System Model

As shown in Fig. 1, we consider an air-to-ground bistatic ISAC system formed by a rotary-wing UAV and a terrestrial sensing receiver. We assume that the UAV hovers at a fixed position $P_0 = (x_0, y_0, H_0)$ and the sensing receiver is located at $P_1 = (x_1, y_1, 0)$. The UAV serves as an aerial access point (AP) to communicate with multiple terrestrial users indexed by set $\mathcal{K} \triangleq \{1, ..., K\}$ and meanwhile, with the aid of the sensing receiver, provide sensing services such as activity detection to multiple targets indexed by $\mathcal{L} \triangleq \{1, ..., L\}$. User $k \in \mathcal{K}$ and target $l \in \mathcal{L}$ are located at $P_{\mathrm{U},k} = (x_k, y_k, 0)$ and $P_{\mathrm{T},l} = (x_l, y_l, z_l)$, respectively, whose positions are known at the UAV and the sensing receiver *a priori*.

The UAV is equipped with a uniform linear array (ULA) composed of N patch antennas, cf. Fig. 1. The 3D orientation of the patch ULA is characterized by its patch axis $\overrightarrow{\boldsymbol{r}_p} \in \mathbb{R}^{3\times 1}$ and array axis $\overrightarrow{\boldsymbol{r}_a} \in \mathbb{R}^{3\times 1}$. We assume that both $\overrightarrow{\boldsymbol{r}_p}$ and $\overrightarrow{\boldsymbol{r}_a}$ can be flexibly adjusted via either rotating the UAV itself or using an additional gimbal device. Meanwhile, each communication user has a single receive antenna and the sensing receiver employs a ULA of M antennas. For convenience, we assume that all receive antennas are isotropic with fixed orientations.

A. Channel Model under 3D Array-Steering

We assume that the elevated UAV can establish LoS links to all communication users and sensing targets [5]. Consequently, the UAV-to-user k channel $\boldsymbol{h}_{\mathrm{c},k} \in \mathbb{C}^{N\times 1}$ is modeled as

$$\boldsymbol{h}_{\mathrm{c},k} = \frac{\sqrt{\beta}}{D_{\mathrm{c},k}} \cdot \boldsymbol{a}_{\mathrm{c},k}, \tag{1}$$

where β is the reference value of path loss at the unit distance, $D_{\mathrm{c},k} \triangleq \sqrt{(x_k - x_0)^2 + (y_k - y_0)^2 + H_0^2}$ denotes the distance between the UAV and user k, and $\boldsymbol{a}_{\mathrm{c},k} \in \mathbb{C}^{N\times 1}$ is the transmit steering vector for user k. Besides, let $\boldsymbol{H}_{\mathrm{s},l} \in \mathbb{C}^{M\times N}$ and $\boldsymbol{H}_{\mathrm{d}} \in \mathbb{C}^{M\times N}$ be the UAV-to-sensing receiver channel matrices due to reflection/scattering at target l and direct signal propagation, which are distinguished in Fig. 1 by blue and red dashed lines, respectively. Following [11], we have

$$\boldsymbol{H}_{\mathrm{s},l} = \frac{\alpha\sqrt{\beta}}{D_{\mathrm{st},l} + D_{\mathrm{sr},l}} \cdot \boldsymbol{a}_{\mathrm{sr},l} \cdot \boldsymbol{a}_{\mathrm{st},l}^H, \tag{2}$$

$$\boldsymbol{H}_{\mathrm{d}} = \frac{\sqrt{\beta}}{D} \cdot \boldsymbol{a}_{\mathrm{dr}} \cdot \boldsymbol{a}_{\mathrm{dt}}^H. \tag{3}$$

In (2), other path loss models can also be applied without changing the problem formulation and solution. Besides, $\boldsymbol{a}_{\mathrm{st},l} \in \mathbb{C}^{N\times 1}$ and $\boldsymbol{a}_{\mathrm{dt}} \in \mathbb{C}^{N\times 1}$ ($\boldsymbol{a}_{\mathrm{sr},l} \in \mathbb{C}^{M\times 1}$ and $\boldsymbol{a}_{\mathrm{dr}} \in \mathbb{C}^{M\times 1}$) denote the transmit (receive) steering vectors for target l and the sensing receiver, respectively. Finally, we assume all targets have the same reflection coefficient $\alpha \in \mathbb{C}$.

Considering the 3D radiation pattern of the patch array, the transmit steering vector $\boldsymbol{a}_{\mathrm{c},k}$ for user k is given by

$$\boldsymbol{a}_{\mathrm{c},k} = \gamma \cdot \mathrm{E}(\theta_{\mathrm{c},k}, \varphi_{\mathrm{c},k}) \cdot \mathrm{A}(\varphi_{\mathrm{c},k}), \tag{4}$$

where $\mathrm{E}(\theta_{\mathrm{c},k}, \varphi_{\mathrm{c},k})$ and $\mathrm{A}(\varphi_{\mathrm{c},k})$ denote the element factor of a patch antenna and the array factor, respectively. $\theta_{\mathrm{c},k}$ and $\varphi_{\mathrm{c},k}$ represent the angles of departure for signal transmission from the UAV to user k with respect to (w.r.t.) the patch axis $\overrightarrow{\boldsymbol{r}_p}$ and the array axis $\overrightarrow{\boldsymbol{r}_a}$, which are also referred to as the elevation angle and azimuth angle of user k, respectively, cf. Fig. 1. Let $\overrightarrow{\boldsymbol{d}}_{\mathrm{c},k} \triangleq (x_k - x_0, y_k - y_0, -H)^T / D_{\mathrm{c},k} \in \mathbb{R}^{3\times 1}$ be the unit direction vector of user k seen from the UAV. We have

$$\theta_{\mathrm{c},k} = \arccos(\overrightarrow{\boldsymbol{d}}_{\mathrm{c},k}^T \cdot \overrightarrow{\boldsymbol{r}_p}) \tag{5}$$

$$\varphi_{\mathrm{c},k} = \arccos(\overrightarrow{\boldsymbol{d}}_{\mathrm{c},k}^T \cdot \overrightarrow{\boldsymbol{r}_a}). \tag{6}$$

Finally, γ in (4) is a normalization factor to limit the total radiated power, such that $\frac{\gamma^2}{4\pi^2}\int_0^\pi\int_0^\pi \mathrm{E}^2(\theta_{\mathrm{c},k}, \varphi_{\mathrm{c},k}) \mathrm{d}\varphi_{\mathrm{c},k}\mathrm{d}\theta_{\mathrm{c},k} = 1$. Assume that all communication users, sensing targets and the sensing receiver are located in the far field of the transmit patch array. Let λ be the carrier wavelength of transmit signals. We consider $\frac{\lambda}{2} \times \frac{\lambda}{2}$ square patch elements, whose element factor $\mathrm{E}(\theta_{\mathrm{c},k}, \varphi_{\mathrm{c},k})$ and array factor $\mathrm{A}(\varphi_{\mathrm{c},k})$) are given by [12]

$$\mathrm{E}(\theta_{\mathrm{c},k}, \varphi_{\mathrm{c},k}) = \sin\theta_{\mathrm{c},k} \cdot \sin\varphi_{\mathrm{c},k}, \tag{7}$$

$$\mathrm{A}(\varphi_{\mathrm{c},k}) = (1, e^{j\frac{2\pi}{\lambda}d\cos\varphi_{\mathrm{c},k}}, \cdots, e^{j(N-1)\frac{2\pi}{\lambda}d\cos\varphi_{\mathrm{c},k}})^T. \tag{8}$$

Here, d is the spacing of adjacent patch elements in the array. Note that the transmit steering vectors $\boldsymbol{a}_{\mathrm{st},l}$ and $\boldsymbol{a}_{\mathrm{dt}}$ can be calculated by replacing $(\theta_{\mathrm{c},k}, \varphi_{\mathrm{c},k})$ in (4) with $(\theta_{\mathrm{st},l}, \varphi_{\mathrm{st},l})$ and $(\theta_{\mathrm{dt}}, \varphi_{\mathrm{dt}})$, respectively.

On the other hand, let $\overrightarrow{\boldsymbol{r}_r} \in \mathbb{R}^{3\times 1}$ be the direction of the ULA with fixed array axis at the sensing receiver. The receive steering vector $\boldsymbol{a}_{\mathrm{sr},l}$ for target l is given as

$$\boldsymbol{a}_{\mathrm{sr},l} = (1, e^{j\frac{2\pi}{\lambda}d\cos\varphi_{\mathrm{sr},l}}, \cdots, e^{j(M-1)\frac{2\pi}{\lambda}d\cos\varphi_{\mathrm{sr},l}})^T, \quad (9)$$

with $\varphi_{\mathrm{sr},l} = \arccos(\overrightarrow{\boldsymbol{d}}_{\mathrm{sr},l}^T \cdot \overrightarrow{\boldsymbol{r}_r})$, and $\overrightarrow{\boldsymbol{d}}_{\mathrm{sr},l} \triangleq (x_1 - x_l, y_1 - y_l, -z_l)^T / D_{\mathrm{sr},l}$ is the unit direction vector of the sensing receiver seen from target l. The receive steering vector $\boldsymbol{a}_{\mathrm{dr}}$ can be modeled by replacing $\varphi_{\mathrm{sr},l}$ in (9) with φ_{dr}.

B. Signal Model for Bistatic ISAC

For the consdiered UAV-aided bistatic ISAC, the UAV transmits a common signal for sensing and communication. The sensing receiver collects the reflected/scattered signals from all targets for e.g. detecting the activity of each target l, whereas this process is impaired by the interference from the UAV. Let $s_k \in \mathbb{C}$ be the data symbol intended for user $k \in \mathcal{K}$. We assume that s_k is a complex Gaussian random variable with zero mean and unit variance, i.e., $s_k \sim \mathcal{CN}(0,1)$. To enable bistatic ISAC, the UAV sends the transmit signal

$$\boldsymbol{s} = \sum\nolimits_{k=1}^{K} \boldsymbol{w}_k \cdot s_k \quad (10)$$

over the patch array, where $\boldsymbol{w}_k \in \mathbb{C}^{N\times 1}$ is the beamforming vector for sending s_k. The received signal at user k is

$$y_k = \boldsymbol{h}_{\mathrm{c},k}^H \cdot \boldsymbol{s} + n_k, \quad (11)$$

where $n_k \in \mathbb{C}$ is the noise at user k, following $n_k \sim \mathcal{CN}(0, \sigma_k^2)$. Then, the received SINR of user k is

$$\mathrm{SINR}_k = \frac{|\boldsymbol{h}_{\mathrm{c},k}^H \boldsymbol{w}_k|^2}{\sum_{m=1,m\neq k}^{K} |\boldsymbol{h}_{\mathrm{c},k}^H \boldsymbol{w}_m|^2 + \sigma_k^2}. \quad (12)$$

Meanwhile, the signal vector $\boldsymbol{x} \in \mathbb{C}^{M\times 1}$ collected at the sensing receiver is given by

$$\boldsymbol{x} = \boldsymbol{H}_{\mathrm{d}} \cdot \boldsymbol{s} + \sum\nolimits_{l=1}^{L} \boldsymbol{H}_{\mathrm{s},l} \cdot \boldsymbol{s} + \boldsymbol{n}_{\mathrm{r}}, \quad (13)$$

where $\boldsymbol{n}_{\mathrm{r}} \in \mathbb{C}^{M\times 1}$ is the receiver noise vector, following $\boldsymbol{n}_{\mathrm{r}} \sim \mathcal{CN}(\boldsymbol{0}, \sigma_{\mathrm{r}}^2 \boldsymbol{I}_M)$. We assume that the UAV and the sensing receiver are perfectly synchronized for the sensing task. Based on knowledge of the target positions, the sensing receiver further applies a matched filter $\boldsymbol{m}_{\mathrm{f},l} = \boldsymbol{a}_{\mathrm{sr},l} / \|\boldsymbol{a}_{\mathrm{sr},l}\|$ on $\boldsymbol{x}$. The resulting filtered signal $z_{\mathrm{f},l}$ of target l is given as

$$\begin{aligned} z_{\mathrm{f},l} =& \boldsymbol{m}_{\mathrm{f},l}^H \cdot \boldsymbol{H}_{\mathrm{s},l} \cdot \boldsymbol{s} + \boldsymbol{m}_{\mathrm{f},l}^H \cdot \boldsymbol{n}_{\mathrm{r}} \\ &+ \underbrace{\boldsymbol{m}_{\mathrm{f},l}^H \cdot (\boldsymbol{H}_{\mathrm{d}} + \sum\nolimits_{m=1,m\neq l}^{L} \boldsymbol{H}_{\mathrm{s},m}) \cdot \boldsymbol{s}}_{\text{interference from the UAV and other sensing targets}}. \end{aligned} \quad (14)$$

Therefore, the received SINR for sensing target l is

$$\mathrm{SINR}_{\mathrm{f},l} = \frac{\sum_{k=1}^{K} |\boldsymbol{b}_l^H \boldsymbol{w}_k|^2}{\sum_{k=1}^{K} |\boldsymbol{c}_l^H \boldsymbol{w}_k|^2 + M\sigma_{\mathrm{r}}^2}, \quad (15)$$

with $\boldsymbol{c}_l \triangleq (\boldsymbol{H}_{\mathrm{d}} + \sum_{m=1,m\neq l}^{L} \boldsymbol{H}_{\mathrm{s},m})^H \boldsymbol{m}_{\mathrm{f},l}$ and $\boldsymbol{b}_l^H \triangleq \boldsymbol{H}_{\mathrm{s},l}^H \boldsymbol{m}_{\mathrm{f},l}$. Note that, as the mutual interference between the sensing targets and the communication users are negligible compared to the LoS signals from the UAV received at the communication users and the sensing receiver (after matched filtering), they are neglected in (12) and (15).

III. Problem Formulation

Based on (12) and (15), the received SINRs of the considered bistatic ISAC system depend on both the transmit beamforming vector $\{\boldsymbol{w}_k\}$ and the orientation $\{\overrightarrow{\boldsymbol{r}_a}, \overrightarrow{\boldsymbol{r}_p}\}$ of the patch array. To best exploit the patch array for bistatic ISAC, we jointly optimize the beamforming and array steering to maximize the minimum received SINR of all targets, while guaranteeing the QoS requirements for communication users. The resulting optimization problem is formulated as

$$\begin{aligned} \underset{\boldsymbol{w}_k, \overrightarrow{\boldsymbol{r}_a}, \overrightarrow{\boldsymbol{r}_p}}{\text{maximize}} \quad & \min_{l} \ \mathrm{SINR}_{\mathrm{f},l} \\ \text{subject to} \quad & \text{C1: } \|\boldsymbol{w}_k\|^2 = P_k, \ k \in \mathcal{K}, \\ & \text{C2: } \mathrm{SINR}_k \geq r_k, \ k \in \mathcal{K}, \\ & \text{C3: } \|\overrightarrow{\boldsymbol{r}_a}\| = 1, \\ & \text{C4: } \|\overrightarrow{\boldsymbol{r}_p}\| = 1, \\ & \text{C5: } \overrightarrow{\boldsymbol{r}_a}^T \cdot \overrightarrow{\boldsymbol{r}_p} = 0. \end{aligned} \quad \text{(P1)}$$

In (P1), constraint C1 limits the transmit power allocated for user k by P_k, where $\sum_{k=1}^{K} P_k = P_{\max}$ and $P_{\max}$ is the total transmit power of the UAV. Here we assume P_ks to be given a priori. However, they can also be optimized using our problem formulation and solution. Meanwhile, C2 guarantees a minimum received SINR of r_k, or equivalently a minimum data rate of $\log_2(1 + r_k)$ in bps/Hz, for user k. Finally, C3, C4 and C5 require $\overrightarrow{\boldsymbol{r}_a}$ and $\overrightarrow{\boldsymbol{r}_p}$ to be orthonormal unit vectors during 3D steering of the patch array, cf. Fig. 1.

Problem (P1) is highly nonconvex, as the objective function and the constraints are all nonconvex. Besides, beamforming vector $\{\boldsymbol{w}_k\}$ and array steering $\{\overrightarrow{\boldsymbol{r}_a}, \overrightarrow{\boldsymbol{r}_p}\}$ are tightly coupled in the objective function and constraint C2, presenting an additional challenge for solving the problem. This type of problem is generally intractable. To tackle problem (P1), we propose a low-complexity suboptimal solution in Section IV.

IV. Problem Solution

By introducing an auxiliary optimization variable η, problem (P1) can be equivalently rewritten as

$$\begin{aligned} \underset{\boldsymbol{w}_k, \eta, \overrightarrow{\boldsymbol{r}_a}, \overrightarrow{\boldsymbol{r}_p}}{\text{maximize}} \quad & \eta \\ \text{subject to} \quad & \mathrm{C1, C2, C3, C4, C5}, \\ & \text{C6: } \mathrm{SINR}_{\mathrm{f},l} \geq \eta, \ l \in \mathcal{L}. \end{aligned} \quad (\overline{\text{P1}})$$

In the following, we propose an iterative proximal BCD algorithm [13] to decompose problem ($\overline{\text{P1}}$) into three subproblems. Each subproblem optimizes one of the three variable blocks, namely $\{\boldsymbol{w}_k, \eta\}$, $\{\overrightarrow{\boldsymbol{r}_a}\}$, and $\{\overrightarrow{\boldsymbol{r}_p}\}$, while keeping the other two blocks of variables fixed. These decomposed subproblems belong to either convex or manifold optimization, for which they can be conveniently solved by off-the-shell solvers. Meanwhile, by introducing proximal and penalty terms, the convergence of the overall BCD algorithm is ensured.

A. Subproblem for Beamforming Optimization

For given array steering $\{\overrightarrow{\boldsymbol{r}_a}, \overrightarrow{\boldsymbol{r}_p}\}$, the beamforming vector $\boldsymbol{w}_k$ and auxiliary variable η can be optimized by solving

$$\underset{\boldsymbol{w}_k, \eta}{\text{maximize}} \quad \eta$$

$$\text{subject to} \quad \mathrm{C1, C2, C6.} \tag{P2}$$

To tackle the nonconvex constraints C1, C2, and C6 in problem (P2), we reformulate it as a semi-definite program (SDP) by defining $\boldsymbol{X}_k \triangleq t\boldsymbol{w}_k^H\boldsymbol{w}_k$ and eliminating $\boldsymbol{w}_k$. Consequently, (P2) can be equivalently rewritten as

$$\begin{aligned} &\underset{\boldsymbol{X}_k,\eta,t}{\text{maximize}} \quad \eta \\ &\text{subject to} \quad \overline{\mathrm{C1}}: \ \mathrm{tr}(\boldsymbol{X}_k) = tP_k, \ k \in \mathcal{K}, \\ &\qquad \overline{\mathrm{C2}}: \sum\nolimits_{m=1,m\neq k}^{K} \mathrm{tr}(\boldsymbol{H}_{\mathrm{c},k}\boldsymbol{X}_m) + t\sigma_k^2 \\ &\qquad\qquad - \frac{1}{r_k}\mathrm{tr}(\boldsymbol{H}_{\mathrm{c},k}\boldsymbol{X}_k) \leq 0, \ k \in \mathcal{K}, \\ &\qquad \overline{\mathrm{C6}}: \ \frac{\sum_{k=1}^{K}\mathrm{tr}(\boldsymbol{B}_l\boldsymbol{X}_k)}{\sum_{k=1}^{K}\mathrm{tr}\left[(\boldsymbol{C}_l + \frac{M\sigma_{\mathrm{r}}^2}{P_{\max}}\boldsymbol{I}_N)\boldsymbol{X}_k\right]} \geq \eta, \ l \in \mathcal{L}, \\ &\qquad \mathrm{C7}: \boldsymbol{X}_k \succeq \boldsymbol{0}, \ \mathrm{C8}: \mathrm{rank}(\boldsymbol{X}_k) = 1, \ k \in \mathcal{K}, \end{aligned} \tag{$\overline{\mathrm{P2}}$}$$

where $\boldsymbol{H}_{\mathrm{c},k} = \boldsymbol{h}_{\mathrm{c},k}\boldsymbol{h}_{\mathrm{c},k}^H$, $\boldsymbol{B}_l = \boldsymbol{b}_l\boldsymbol{b}_l^H$, and $\boldsymbol{C}_l = \boldsymbol{c}_l\boldsymbol{c}_l^H$. Note that $\overline{\mathrm{C1}}$ and C7 imply $t \geq 0$ (or $t > 0$ provided $\boldsymbol{X}_k \neq 0$ for some $k \in \mathcal{K}$).

In problem ($\overline{\mathrm{P2}}$), constraints $\overline{\mathrm{C6}}$ and C8 are still nonconvex. We tackle this challenge by applying the Charnes-Cooper transformation to $\overline{\mathrm{C6}}$ and relaxing C8. The resulting problem becomes a convex SDP [14], which is given as

$$\begin{aligned} &\underset{\boldsymbol{X}_k,\eta,t}{\text{maximize}} \quad \eta \\ &\text{subject to} \quad \overline{\mathrm{C1}}, \overline{\mathrm{C2}}, \mathrm{C7}, \\ &\qquad \widetilde{\mathrm{C6}}\mathrm{a}: \sum\nolimits_{k=1}^{K} \mathrm{tr}(\boldsymbol{B}_l\boldsymbol{X}_k) \geq \eta, \ l \in \mathcal{L}, \\ &\qquad \widetilde{\mathrm{C6}}\mathrm{b}: \sum\nolimits_{k=1}^{K} \mathrm{tr}\left[(\boldsymbol{C}_l + \frac{M\sigma_{\mathrm{r}}^2}{P_{\max}}\boldsymbol{I}_N)\boldsymbol{X}_k\right] = 1, \ l \in \mathcal{L}. \end{aligned} \tag{$\widetilde{\mathrm{P2}}$}$$

Note that the equality constraints $\overline{\mathrm{C1}}$ and $\widetilde{\mathrm{C6}}\mathrm{b}$ are feasible whenever $K\frac{N(N+1)}{2} > K + L$. ($\widetilde{\mathrm{P2}}$) can be efficiently solved using the available solvers, such as CVX [15]. In general, due to the relaxation of C8, the obtained optimal solution $\boldsymbol{X}_k^*$ may not be of rank one. In such case, Gaussian randomization or eigenvalue decomposition techniques can be applied to recover the optimal $\boldsymbol{w}_k^*$ from $\boldsymbol{X}_k^*$ [15]. However, we observe in our simulations that, $\boldsymbol{X}_k^*$ consistently satisfies C8, particularly through adopting the equality constraint specified in C1 (rather than rewriting it into an inequality form). A similar result with strict proof has also been reported in [16].

B. Subproblem for Optimizing 3D Array Steering

We now optimize the array steering $\overrightarrow{\boldsymbol{r}_a}$ for given $\{\boldsymbol{w}_k, \eta\}$ and $\overrightarrow{\boldsymbol{r}_p}$, which is formulated as

$$\begin{aligned} &\underset{\overrightarrow{\boldsymbol{r}_a}}{\text{maximize}} \quad \eta \\ &\text{subject to} \quad \mathrm{C2, C3, C5, C6.} \end{aligned} \tag{P3}$$

Exploiting the symmetry between $\overrightarrow{\boldsymbol{r}_a}$ and $\overrightarrow{\boldsymbol{r}_p}$, the subproblem of optimizing $\overrightarrow{\boldsymbol{r}_p}$ can be tackled by simply interchanging $\overrightarrow{\boldsymbol{r}_a}$ and $\overrightarrow{\boldsymbol{r}_p}$ in the presented solution, whose formulation and solution are thus ignored due to limited page space.

Note that, by fixing vector $\overrightarrow{\boldsymbol{r}_p}$, all vectors $\overrightarrow{\boldsymbol{r}_a}$ satisfying constraints C3 and C5 form a unit circle manifold within the null-space of $\overrightarrow{\boldsymbol{r}_p}$, denoted by $\mathcal{M}(\overrightarrow{\boldsymbol{r}_p})$. To exploit this special geometry, we consider solving (P3) by manifold optimization. In particular, we first rewrite (P3) into a standard manifold optimization problem,

$$\underset{\overrightarrow{\boldsymbol{r}_a} \in \mathcal{M}(\overrightarrow{\boldsymbol{r}_p})}{\text{minimize}} \quad g(\overrightarrow{\boldsymbol{r}_a}), \tag{$\overline{\mathrm{P3}}$}$$

where $g(\cdot)$ is a smooth real-valued function defined on $\mathcal{M}(\overrightarrow{\boldsymbol{r}_p})$. This is achieved by imposing constraints C2 and C6 only implicitly, i.e., via adding a log-sum-exp penalty term into the objective function such that

$$\begin{aligned} g(\overrightarrow{\boldsymbol{r}_a}) \triangleq &-\eta + \rho \cdot \big[\sum\nolimits_{k=1}^{K} u \log(1 + e^{\frac{r_k - \mathrm{SINR}_k}{u}}) \\ &+ \sum\nolimits_{l=1}^{L} u \log(1 + e^{\frac{\eta - \mathrm{SINR}_{\mathrm{f},l}}{u}})\big] + q \cdot \|\overrightarrow{\boldsymbol{r}_a} - \overrightarrow{\boldsymbol{r}_a}'\|^2. \end{aligned} \tag{16}$$

Here, $q \geq 0$ and $\rho > 0$ are penalty factors, and $u > 0$ is a factor to control the smoothness of the penalty term. Note that, with large ρ and small u, the log-sum-exp function closely approximates the l_1-norm penalty term $\rho \cdot \left[\sum_{k=1}^{K}\max\{0, r_k - \mathrm{SINR}_k\} + \sum_{l=1}^{L}\max\{0, \eta - \mathrm{SINR}_{\mathrm{f},l}\}\right]$. The latter is equivalent to C2 and C6. In (16), $\overrightarrow{\boldsymbol{r}_a}'$ represents the direction vector obtained in the last iteration. Moreover, $q \cdot \|\overrightarrow{\boldsymbol{r}_a} - \overrightarrow{\boldsymbol{r}_a}'\|^2$ is a quadratic proximal term, which can connvexify problem ($\overline{\mathrm{P3}}$) and prevent substantial deviations between the optimal solution of ($\overline{\mathrm{P3}}$) and $\overrightarrow{\boldsymbol{r}_a}'$ to improve the convergence of the solution.

Problem ($\overline{\mathrm{P3}}$) can already be solved by manifold optimization methods such as the Riemannian conjugate gradient (RCG) algorithm, which is available in off-the-shelf solvers such as pymanopt [17]. In fact, we can further simplify problem ($\overline{\mathrm{P3}}$) via suitable transformation. Specifically, let $\boldsymbol{e} = [\boldsymbol{e}_1, \boldsymbol{e}_2] \in \mathbb{R}^{3\times 2}$ be the orthonormal basis for the null-space of $\overrightarrow{\boldsymbol{r}_p}$. We can express the 3D vector $\overrightarrow{\boldsymbol{r}_a} \in \mathcal{M}(\overrightarrow{\boldsymbol{r}_p})$ as

$$\overrightarrow{\boldsymbol{r}_a} = \boldsymbol{e} \cdot \boldsymbol{\gamma}_a, \tag{17}$$

for $\boldsymbol{\gamma}_a$ lying on a two-dimensional (2D) manifold, $\mathcal{M}(\boldsymbol{\gamma}_a) \triangleq \{\boldsymbol{\gamma}_a \in \mathbb{R}^{2\times 1} \mid \|\boldsymbol{\gamma}_a\| = 1\}$. Now substituting the optimization variable $\overrightarrow{\boldsymbol{r}_a}$ in ($\overline{\mathrm{P3}}$) with $\boldsymbol{\gamma}_a$, ($\overline{\mathrm{P3}}$) is reformulated as

$$\underset{\boldsymbol{\gamma}_a \in \mathcal{M}(\boldsymbol{\gamma}_a)}{\text{minimize}} \quad g(\boldsymbol{e} \cdot \boldsymbol{\gamma}_a), \tag{$\widetilde{\mathrm{P3}}$}$$

which has a lower solution complexity than ($\overline{\mathrm{P3}}$).

The overall algorithm solves problem ($\overline{\mathrm{P1}}$) by iteratively optimizing the three variable blocks $\{\boldsymbol{w}_k, \eta\}$, $\{\overrightarrow{\boldsymbol{r}_a}\}$, $\{\overrightarrow{\boldsymbol{r}_p}\}$ until reaching convergence, which is summarized in Algorithm 1. The solution for ($\widetilde{\mathrm{P3}}$) employs the Riemannian exact penalty method via smoothing (REPMS) and the optimal array steering $\overrightarrow{\boldsymbol{r}_a}^*$ can be recovered by (17). While solving ($\widetilde{\mathrm{P3}}$) or ($\overline{\mathrm{P3}}$), the penalty factor ρ should be carefully selected, as problem ($\widetilde{\mathrm{P3}}$) may become ill-conditioned with an excessively large ρ, impeding the algorithm's convergence. In Algorithm 1, we overcome this issue by setting a small initial value for ρ and gradually increasing ρ.

V. Simulation Results

In this section, we evaluate the performance of the proposed scheme for UAV-aided bistatic ISAC via simulations. The UAV

Algorithm 1 Proximal BCD Algorithm to Solve $(\overline{\text{P1}})$

Input: Initial penalty weight ρ_0, initial smoothing factor u_0, initial proximal term q_0, $\delta_\rho > 1$, $0 < \delta_u < 1$, $\delta_q > 1$, $u_{\min}$, $\rho_{\max}$, $q_{\max}$, REPMS stopping threshold ϵ_1, BCD stopping threshold ϵ_2, d_1, d_2, $t_1 = 0$, $t_2 = 0$, initial beamforming vectors $\boldsymbol{W}_0 = [\boldsymbol{w}_{1,0}, \cdots, \boldsymbol{w}_{K,0}]$, initial array steering $\overrightarrow{\boldsymbol{r}}_{a,0}$ and $\overrightarrow{\boldsymbol{r}}_{p,0}$.

Output: Optimal $\boldsymbol{W}^*$, $\overrightarrow{\boldsymbol{r}_a}^*$ and $\overrightarrow{\boldsymbol{r}_p}^*$

1: **while** $d_2 > \epsilon_2$ **do**
2: Optimize subproblem $(\widetilde{\text{P2}})$, and get $\boldsymbol{W}^*_{t_2+1}$ and $\eta^*_{t_2+1}$.
3: Set $t_1 = 0$, $\rho_{t_1} = \rho_0$, $u_{t_1} = u_0$ and $d_1 = 2\epsilon_1$.
4: **while** $d_1 > \epsilon_1$ **do**
5: Optimize problem $(\widetilde{\text{P3}})$ with q_{t_2}, ρ_{t_1} and u_{t_1} by RCG manifold optimization, and obtain $\boldsymbol{\gamma}^*_{a,t_1+1}$.
6: $\rho_{t_1+1} \leftarrow \min\{\delta_\rho \rho_{t_1}, \rho_{\max}\}$.
7: $u_{t_1+1} \leftarrow \max\{\delta_u u_{t_1}, u_{\min}\}$.
8: $d_1 \leftarrow \|\boldsymbol{\gamma}^*_{a,t_1+1} - \boldsymbol{\gamma}^*_{a,t_1}\|$ and $t_1 \leftarrow t_1 + 1$.
9: **end while**
10: Calculate $\overrightarrow{\boldsymbol{r}}^*_{a,t_2+1}$ with (17).
11: Calculate $\overrightarrow{\boldsymbol{r}}^*_{p,t_2+1}$ with the same steps (3)–(11).
12: $q_{t_2+1} \leftarrow \min\{\delta_q q_{t_2}, q_{\max}\}$
13: $d_2 \leftarrow |\eta^*_{t_2+1} - \eta^*_{t_2}|$ and $t_2 \leftarrow t_2 + 1$.
14: **end while**

hovers at position $P_0 = (0, 0, 20)$ m for both communicating with $K = 2$ users and sensing multiple targets in the 30 GHz frequency band, where the wavelength is $\lambda = 10$ mm. The UAV is equipped with a rotatable ULA of $N = 8$ patch antennas, where the neighboring patch elements are separated by $d = \lambda/2$. The maximal transmit power of the UAV is $P_{\max} = 1$ W and is equally shared by two users, i.e., $P_1 = P_2 = P_{\max}/2$, for fair resource allocation. A sensing receiver located at $P_1 = (0, 200, 0)$ m employs a fixed ULA of $M = 8$ isotropic antennas to collect the signals scattered from all targets. User 1 and 2 are located at $P_{\text{U},1} = (300, 100, 0)$ m and $P_{\text{U},2} = (-510, 600, 0)$ m, respectively. Each user requires a minimum SINR of $r_k = 1$ or a minimum data rate of $\log_2(1 + r_k) = 1$ bps/Hz. The noise power σ_k^2, $k \in \mathcal{K}$ and σ_r^2 are both assumed to be 10^{-12} W. Finally, The path loss coefficient and the reflection coefficient are set as $\beta = 10^{-6}$ and $\alpha = 0.5$, respectively.

Meanwhile, for the proposed BCD algorithm, the upper bound of penalty factor $\rho_{\max}$ and the lower bound of smoothing factor $u_{\min}$ are set to 10^6 and 10^{-6}, respectively. During array steering optimization, the initial array steering of the transmitter is set to $\overrightarrow{\boldsymbol{r}}_{a,0} = (1, 0, 0)^T$ and $\overrightarrow{\boldsymbol{r}}_{p,0} = (0, 0, 1)^T$. By contrast, the array steering of the sensing receiver is fixed as $\overrightarrow{\boldsymbol{r}_r} = (1, 0, 0)^T$. For performance comparison, we consider the following schemes as benchmarks,

- *Baseline Scheme 1:* The UAV employs a non-rotatable ULA of patch elements with fixed array steering $\overrightarrow{\boldsymbol{r}_a} = (1, 0, 0)^T$ and $\overrightarrow{\boldsymbol{r}_p} = (0, 0, 1)^T$. Only the transmit beamforming is optimized.
- *Baseline Scheme 2:* The UAV employs a rotatable ULA of isotropic elements. The array steering and transmit beamforming are jointly optimized.
- *Baseline Scheme 3:* The UAV employs a non-rotatable ULA with isotropic elements with fixed array steering $\overrightarrow{\boldsymbol{r}_a} = (1, 0, 0)^T$. Only transmit beamforming is optimized.

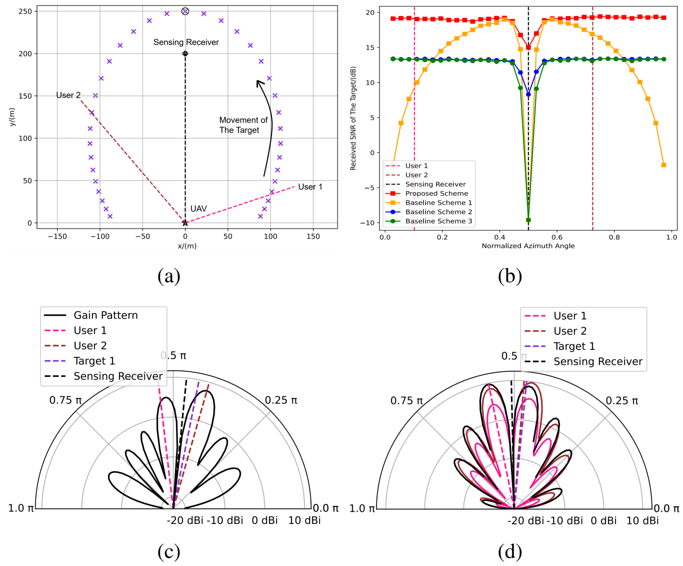

Fig. 2. (a) System settings for a moving target, (b) Performance comparison of considered schemes, and Optimized transmit beampattern gains of (c) Baseline Scheme 2 and (d) Proposed Scheme.

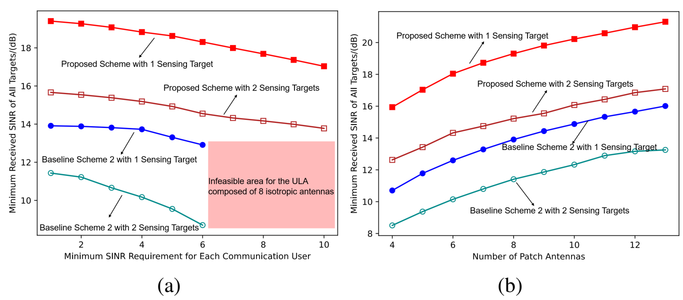

Fig. 3. Performance comparison of Proposed Scheme and Baseline Scheme 2 for (a) Increasing minimum required data rates of users and (b) Increasing number of transmit antennas.

For Baseline Schemes 1-3, transmit beamforming and/or array steering are also optimized using Algorithm 1.

We first consider a single moving sensing target, i.e., $L = 1$. As shown in Fig. 2(a), the target travels along a horizontal elliptic trajectory (indicated by violet crosses) at a fixed height of 20 m, where the foci of the ellipse coincide with the UAV and the sensing receiver. The total length of the UAV-to-sensing receiver path via the target, referred to as a sensing path, is approximately 300 m and remains unchanged during the target's movement. Meanwhile, Fig. 2(b) shows the received SINR (in decibels) of the target during its movement for different schemes, where the azimuth angles of the communication users and the sensing receiver w.r.t. the *initial* array steering $\overrightarrow{\boldsymbol{r}_a} = (1, 0, 0)^T$ are illustrated in dashed lines. We observe that, by using a non-rotatable ULA of isotropic and patch antennas in Baseline Schemes 1 and 3, the target's received SINR significantly decreases when it moves to the same azimuth angle as the sensing receiver, i.e., when it is in the position marked by the circle in Fig. 2(a). This result is expected as the sensing path overlaps with the direct UAV-to-sensing receiver path, or direct path for short, in the horizontal plane, and beamforming alone can not mitigate the strong direct-path interference. However, both the Baseline Scheme 2 and the Proposed Scheme can leverage joint transmit beamforming and array steering to mitigate the direct-path interference, for which their received SINR for the target only decreases slightly.

For further insights into the results in Fig. 2(b), Figs. 2(c) and 2(d) depict the optimized transmit beampattern gains for the rotatable ULA of isotropic and patch antennas, respectively, when the target and the sensing receiver share the same azimuth angle. The dashed lines represent the azimuth angle of the target, communication users and the sensing receiver relative to the *optimized* array orientation vector $\overrightarrow{\boldsymbol{r}_a}^*$. We observe from Figs. 2(c) and 2(d) that the rotatable ULAs can exploit array steering to successfully separate the target and sensing receiver into different azimuth angles, by serving both the target and user 2 within one beam. As a result, the impact of direct-path interference is mitigated at the sensing receiver. In Fig. 2(a), we also observe that the proposed scheme achieves an approximately 7 dB higher received SINR than Baseline Scheme 2 during the target's movement, thanks to the high directivity of patch antennas. However, the Baseline Scheme 1 employing a non-rotatable ULA of patch antennas may perform worse than the Baseline Scheme 3 with a non-rotatable ULA of isotropic antennas when the azimuth angle of the target relative to the fixed array steering $\overrightarrow{\boldsymbol{r}_a} = (1, 0, 0)^T$ approaches 0 or π. This is because the element factor of patch antennas will be nulled at the azimuth angle of 0 and π. These results highlight the importance of array steering for deploying ULAs of directional antennas in practical ISAC systems.

Finally, Figs. 3(a) and 3(b) compare the sensing performance of the Proposed Scheme and Baseline Scheme 2 for varying minimum SINRs required by the users and varying number of transmit antennas, respectively, where we consider $L = 1$ and $L = 2$ targets for each configuration. The targets are located at $P_{\mathrm{T},1} = (100, 100, 15)$ m and $P_{\mathrm{T},2} = (-150, 75, 15)$ m. We observe that, for both the Proposed Scheme and the Baseline Scheme 2, the minimum received sensing SINR of the targets dramatically decreases with the number of targets, as each newly added target may contribute additional interference to other targets. Fig. 3(a) shows that the minimum received sensing SINRs of both the Proposed Scheme and the Baseline Scheme 2 decrease as the minimum SINRs/data rates required for communication increase, due to the inherent trade-off between sensing and communication under a given transmit power budget. However, the Baseline Scheme 2 fails to meet the minimum communication SINR requirements beyond 6, or a minimum data rate exceeding 2.81 bps/Hz, due to the small antenna gain of the isotropic antennas. Besides, Figure 3(b) shows that the sensing performance improves as the number of transmit antennas increases, due to the increased spatial DoFs available for beamforming. Figs. 3(a) and 3(b) also reveal that the Proposed Scheme always achieves the best performance in the UAV-aided bistatic ISAC for the considered parameter settings. It is particularly effective in scenarios involving strong direct-path interference, or when the communication users demand high data rates. Moreover, since the Proposed Scheme already achieves significantly high performance even with a small number of antennas, it also has the potential for applications in UAVs with limited SWAP.

VI. Conclusions

In this paper, we employed a rotatable ULA of patch antennas for signal transmission in UAV-aided bistatic ISAC. We formualted a highly nonconvex problem to jointly optimize transmit beamforming and 3D array-steering for maximizing the minimum received SINR of all targets at the sensing receiver while guaranteeing QoS for each communcation user. Exploiting the underlying structure in formulated problem, we decomposed it into convex and manifold optimization subproblems and further solved them with a low-complexity the proximal BCD method. Simulation results showed that with joint beamforming and array steering, the rotatable ULA of patch antennas can achieve superior performance in UAV-aided bistatic ISAC, even in scearios with limited number of transmit antennas and strong direct-path interference.

References

[1] O. Rezaei, M. M. Naghsh, et al., "Resource Allocation for UAV-Enabled Integrated Sensing and Communication (ISAC) via Multi-Objective Optimization," in *Proc. IEEE ICASSP*, pp. 1-5, 2023.

[2] M. A. Khan, et al., "Swarm of UAVs for Network Management in 6G: A Technical Review," *IEEE Trans. Netw. Serv. Manag.*, vol. 20, no. 1, pp. 741-761, March 2023.

[3] J. Mu, R. Zhang, et al., "UAV Meets Integrated Sensing and Communication: Challenges and Future Directions," *IEEE Commun. Mag.*, vol. 61, no. 5, pp. 62-67, May 2023.

[4] K. Meng, Q. Wu, et al., "UAV Trajectory and Beamforming Optimization for Integrated Periodic Sensing and Communication," *IEEE Wireless Commun. Lett.*, vol. 11, no. 6, pp. 1211-1215, Jun. 2022.

[5] K. Meng, Q. Wu, et al., "Throughput Maximization for UAV-Enabled Integrated Periodic Sensing and Communication," *IEEE Trans. Wireless Commun.*, vol. 22, no. 1, pp. 671-687, Jan. 2023.

[6] Q. Wu, Y. Zeng, et al., "Joint Trajectory and Communication Design for Multi-UAV Enabled Wireless Networks," *IEEE Trans. Wireless Commun.*, vol. 17, no. 3, pp. 2109-2121, Mar. 2018.

[7] Pei, F., Xiang, L., et al., "Joint Optimization of Beamforming and 3D Array-Steering for UAV-Aided ISAC," in *IEEE Int. Conf. Commun. (ICC)*, Denver, Colorado, 2024.

[8] Xiang, L., Pei, F., et al., "Joint Optimization of Beamforming and 3D Array Steering for Multi-antenna UAV Communications," in *Proc. IEEE WCNC*, Dubai, VAE, 2024.

[9] Q. Zhao, A. Tang, et al., "Joint Transmit and Receive Beamforming for Integrated Bistatic Radar Sensing and MU-MIMO Communications," in *Proc. IEEE VTC*, Hong Kong, 2023, pp. 1-6.

[10] M. A. Attalah, T. Laroussi, et al., "Adaptive filters for direct path and multipath interference cancellation: Application to FM-RTL-SDR based Passive Bistatic Radar," in *Proc. IEEE SETIT*, Hammamet, Tunisia.

[11] Q. Wu, S. Zhang, et al., "Intelligent Reflecting Surface-Aided Wireless Communications: A Tutorial," *IEEE Trans. Wireless Commun.*, vol. 69, no. 5, pp. 3313-3351, May 2021.

[12] C. A. Balanis, *Antenna Theory: Analysis and Design*. 4th ed, 2016.

[13] J. Bolte, S. Sabach and M. Teboulle, "Proximal alternating linearized minimization for nonconvex and nonsmooth problems," *Mathematical Programming*, vol. 146, no. 1-2, pp. 459-494, Oct. 2014.

[14] Q. Li, et al, "Constant Modulus Secure Beamforming for Multicast Massive MIMO Wiretap Channels," *IEEE Trans. Inf. Forensics Secur.*, vol. 15, pp. 264-275, 2020.

[15] D. P. Palomar and Y. C. Eldar, *Convex Optimization in Signal Processing and Communications,* 2009.

[16] Z. He, et al, "Full-Duplex Communication for ISAC: Joint Beamforming and Power Optimization," *IEEE J. Sel. Areas Commun.*, vol. 41, no. 9, pp. 2920-2936, Sept. 2023.

[17] P.-A. Absil, R. Mahony and R. Sepulchre, *Optimization Algorithms on Matrix Manifolds.* Princeton University Press, 2009.

[18] C. Liu and N. Boumal, *Simple algorithms for optimization on Riemannian manifolds with constraints*. Jan. 2019.